Supporting Information

Novel "Turn-Off" and "Turn-On" Fluorescent Responses for Zr^{4+} Enabled by Rare-Earth Coordination Polymers Based on the 2,5-Dihydroxyterephthalic Acid Ligand

Yan Liu,[‡a] Wanting Chen,[‡a] Bobi Zheng[a], Han Xu,[b] and Jumei Tian[*a]

[a] Engineering Research Center of Stomatological Biomaterials, Fujian Province University, School of Stomatology of Xiamen Medical College, Xiamen, Fujian 361023, China.

[b] Yunnan Key Laboratory of Pharmacology for Natural Products, School of Pharmaceutical Science, Kunming Medical University, Kunming, Yunnan 650500, China.

[‡] Yan Liu and Wanting Chen contributed equally to this work.

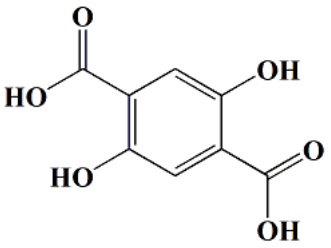

2,5-Dihydroxyterephthalic acid

(H_4dhtp)

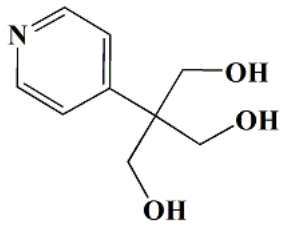

4-(tris(hydroxymethyl)methyl)pyridine

(4-thmpyH_3)

Scheme S1 The ligands using in this system. 2,5-Dihydroxyterephthalic acid (abbreviated H_4dhtp); 4-(tris(hydroxymethyl)methyl)pyridine (abbreviated 4-thmpyH_3).

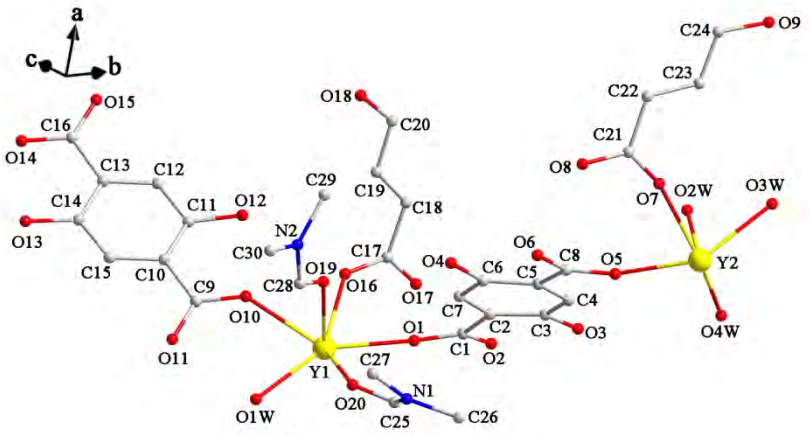

Fig. S1 Ball-and-stick representation of the asymmetric unit for complex **2**. Hydrogen atoms and the crystalline solvent (N, N-dimethylformamide (DMF) and H_2O) have been omitted for clarity.

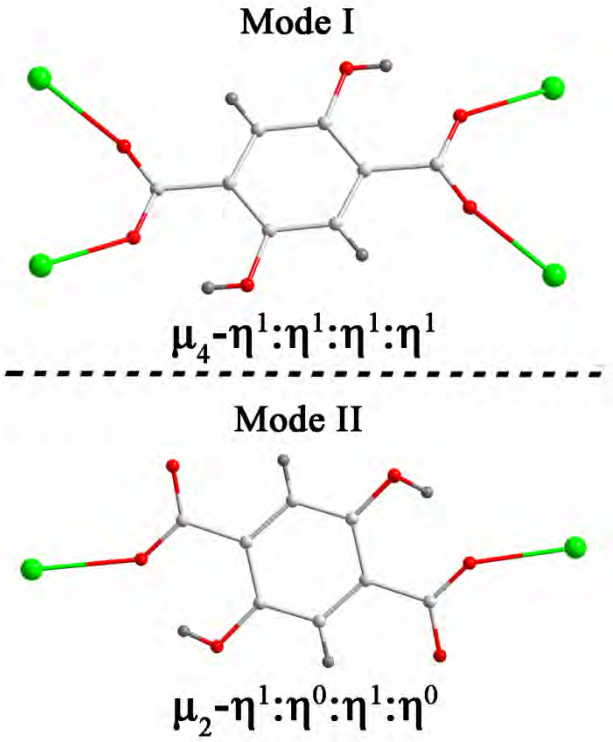

Fig. S2 The coordination modes of the H_2dhtp^{2-} linker for **1**.

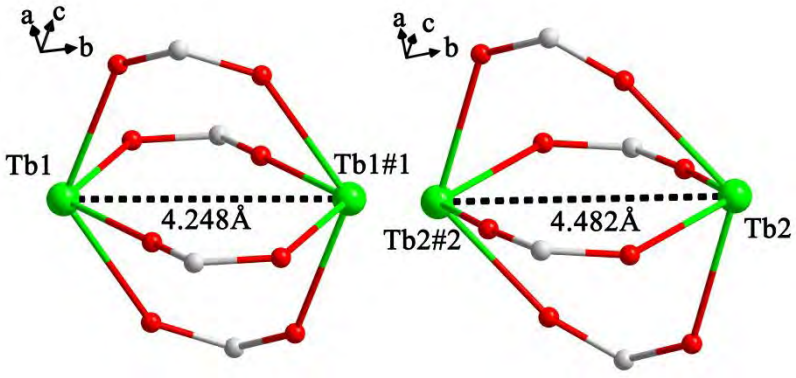

Fig. S3 The H_2dhtp^{2-} ligands of **1** through coordination mode I. #1: -x,1-y,1-z; #2: 1-x,1-y,-z.

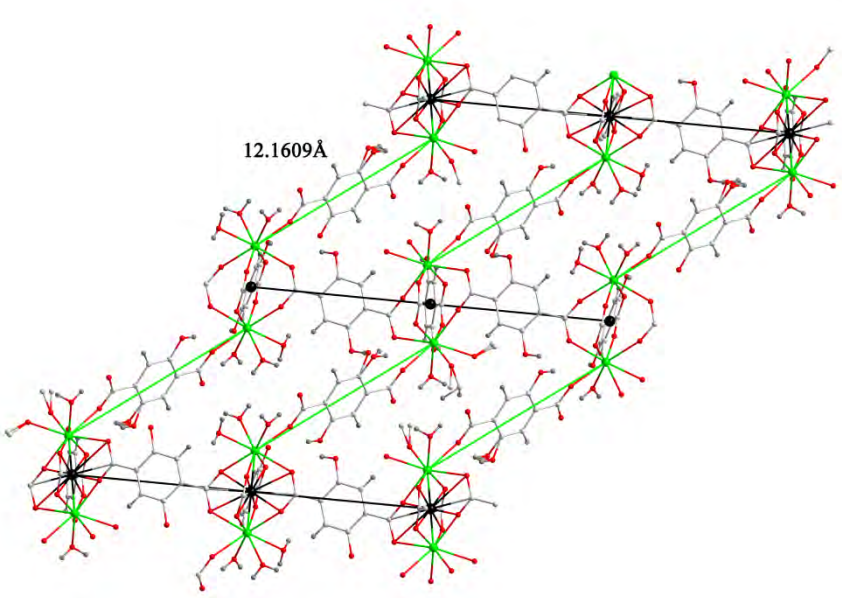

Fig. S4 The view of the 3D framework structure linked the diamond shaped layer by H_2dhtp^{2-} ligand through mode II along *a* axle for **1**.

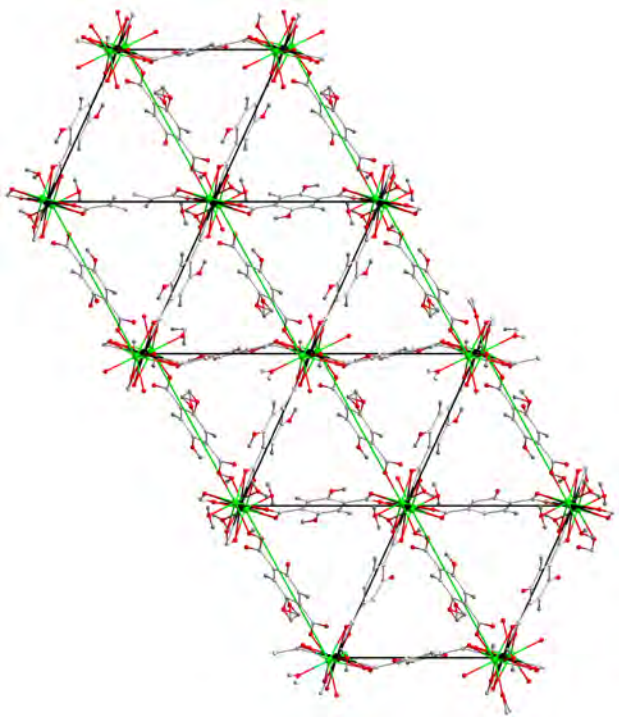

Fig. S5 The view of the 3D framework structure linked the diamond shaped layer by H_2dhtp^{2-} ligand through mode II along *b* axle for **1**.

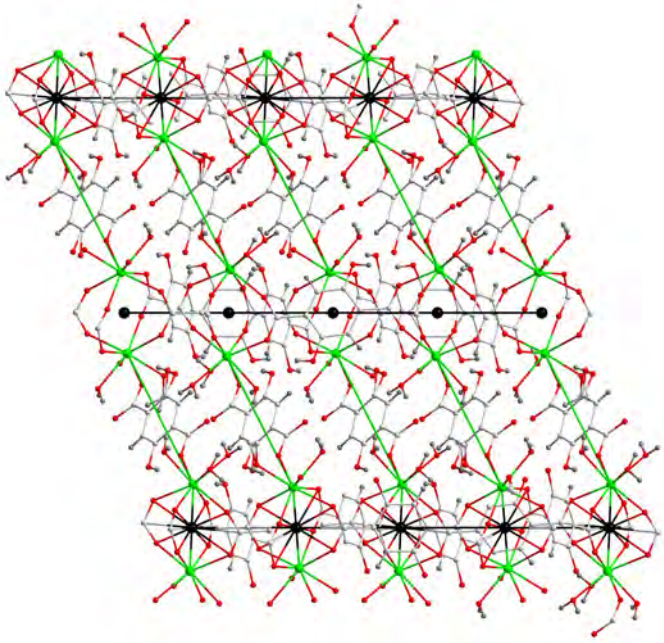

Fig. S6 The view of the 3D framework structure linked the diamond shaped layer by H_2dhtp^{2-} ligand through mode II along *c* axle for **1**.

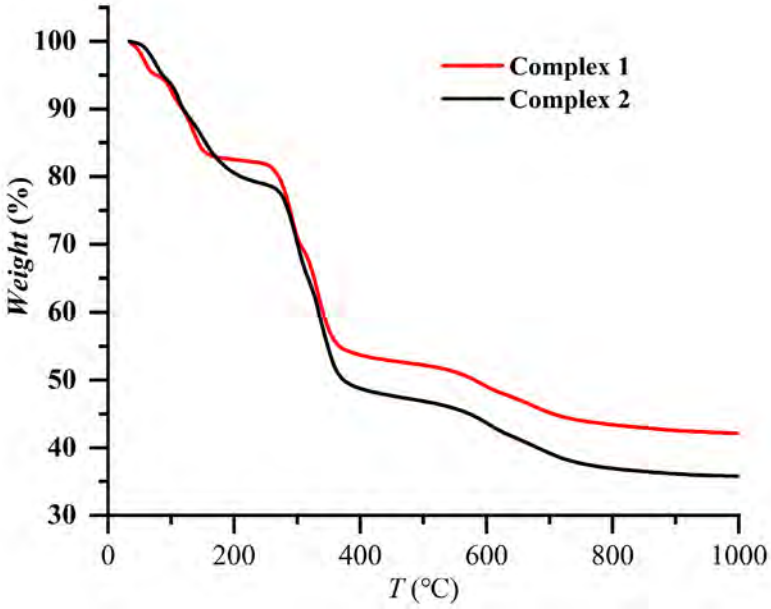

Fig. S7 The TGA curves of **1** (red) and **2** (black).

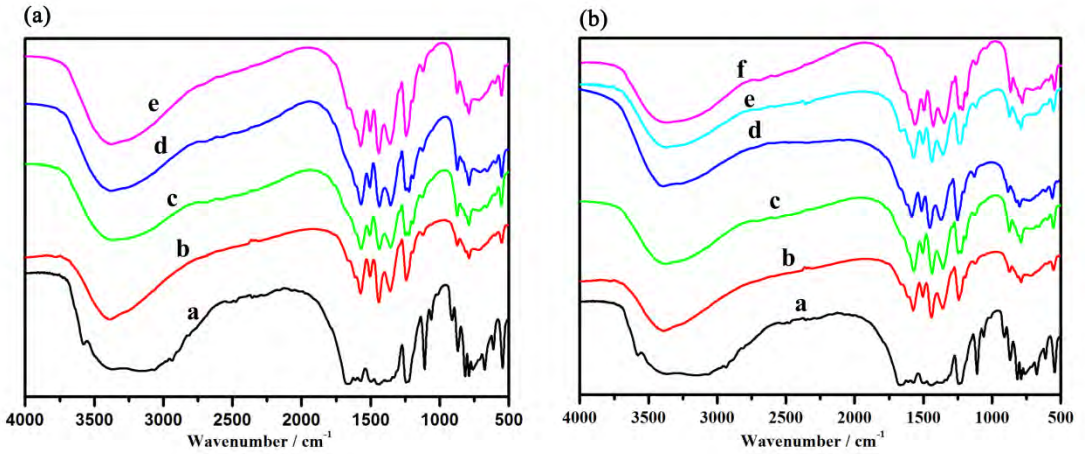

Fig. S8 The IR spectrums for **1** in KBr pellets from 4000 cm^{-1} to 450 cm^{-1}. (a) a: the as-synthesised sample; b: after dispersed in water with ultrasound for 30 min; c: after soaking in 10μM Fe^{3+} solution; d: after soaking in 100μM Fe^{3+} solution; e: after soaking in 400μM Fe^{3+} solution. (b) a: as-synthesised sample; b: after dispersed in water with ultrasound for 30 min; c: after soaking in 5μM Zr^{4+} solution; d: after soaking in 100μM Zr^{4+} solution; e: after soaking in 400μM Zr^{4+} solution; f: after soaking in 700μM Zr^{4+} solution.

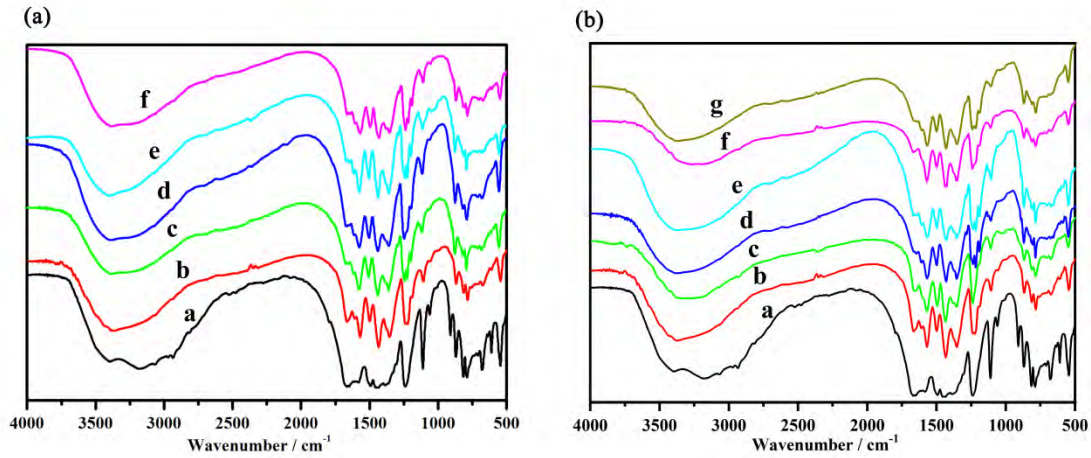

Fig. S9 The IR spectrums for **2** in KBr pellets from 4000 cm^{-1} to 450 cm^{-1}. (a) a: the as-synthesised sample; b: after dispersed in water with ultrasound for 30 min; c: after soaking in 23.8μM Fe^{3+} solution; d: after soaking in 47.6μM Fe^{3+} solution; e: after soaking in 95.2μM Fe^{3+} solution; f: after soaking in 381μM Fe^{3+} solution. (b) a: the as-synthesised sample; b: after dispersed in water with ultrasound for 30 min; c: after soaking in 10μM Zr^{4+} solution; d: after soaking in 60μM Zr^{4+} solution; e: after soaking in 90μM Zr^{4+} solution; f: after soaking in 300μM Zr^{4+} solution; g: after soaking in 500μM Zr^{4+} solution.

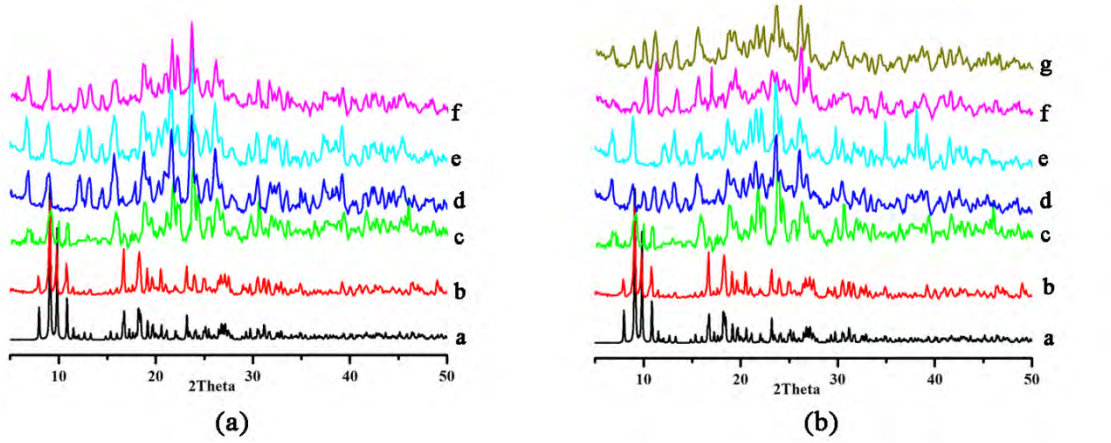

Fig. S10 The Powder X-ray diffraction (PXRD) patterns for **1**. (a) a: the simulated pattern from single crystal X-ray data; b: the experimental pattern at room temperature; c: after dispersed in water with ultrasound for 30 min; d: after soaking in 10μM Fe^{3+} solution; e: after soaking in 100μM Fe^{3+} solution;f: after soaking in 400μM Fe^{3+} solution. (b) a: the simulated pattern from single crystal X-ray data; b: the experimental pattern at room temperature; c: after dispersed in water with ultrasound for 30 min; d: after soaking in 5μM Zr^{4+} solution; e: after soaking in

100μM Zr^{4+} solution;f: after soaking in 400μM Zr^{4+} solution; g: after soaking in 700μM Zr^{4+} solution.

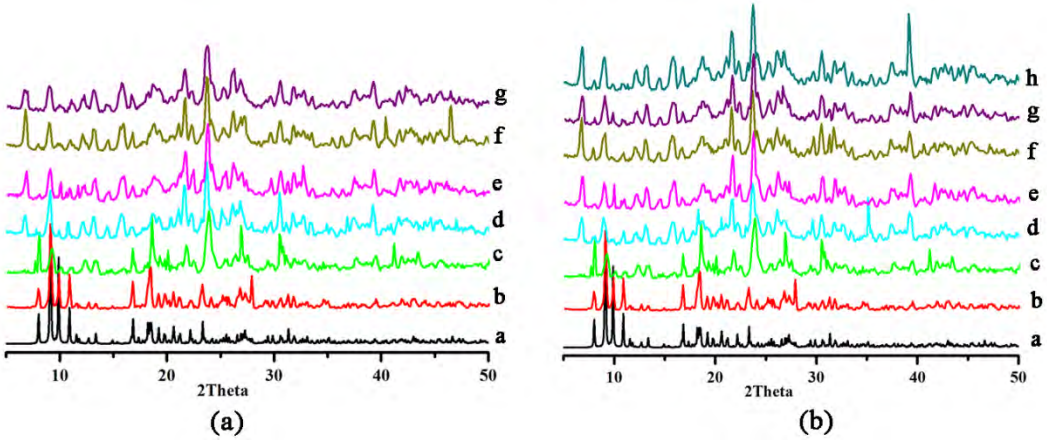

Fig. S11 The Powder X-ray diffraction (PXRD) patterns for **2**. (a) a: the simulated pattern from single crystal X-ray data; b: the experimental pattern at room temperature; c: after dispersed in water with ultrasound for 30 min; d: after soaking in 23.8μM Fe^{3+} solution; e: after soaking in 47.6μM Fe^{3+} solution; f: after soaking in 95.2μM Fe^{3+} solution; g: after soaking in 381μM Fe^{3+} solution. (b) a: the simulated pattern from single crystal X-ray data; b: the experimental pattern at room temperature; c: after dispersed in water with ultrasound for 30 min; d: after soaking in 10μM Zr^{4+} solution; e: after soaking in 60μM Zr^{4+} solution; f: after soaking in 90μM Zr^{4+} solution; g: after soaking in 300μM Zr^{4+} solution; h: after soaking in 500μM Zr^{4+} solution.

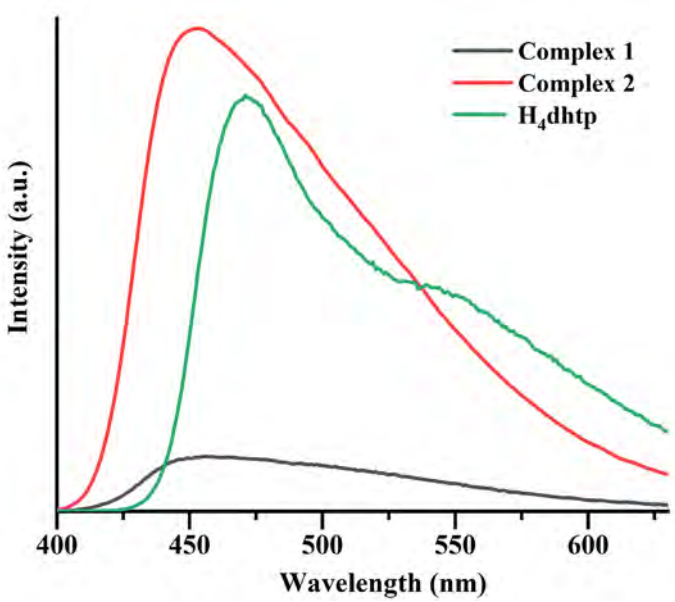

Fig. S12 The solid-state emission spectra of H_4dhtp, complex **1** and complex **2** at excitation of 380, 330, and 320 nm, respectively.

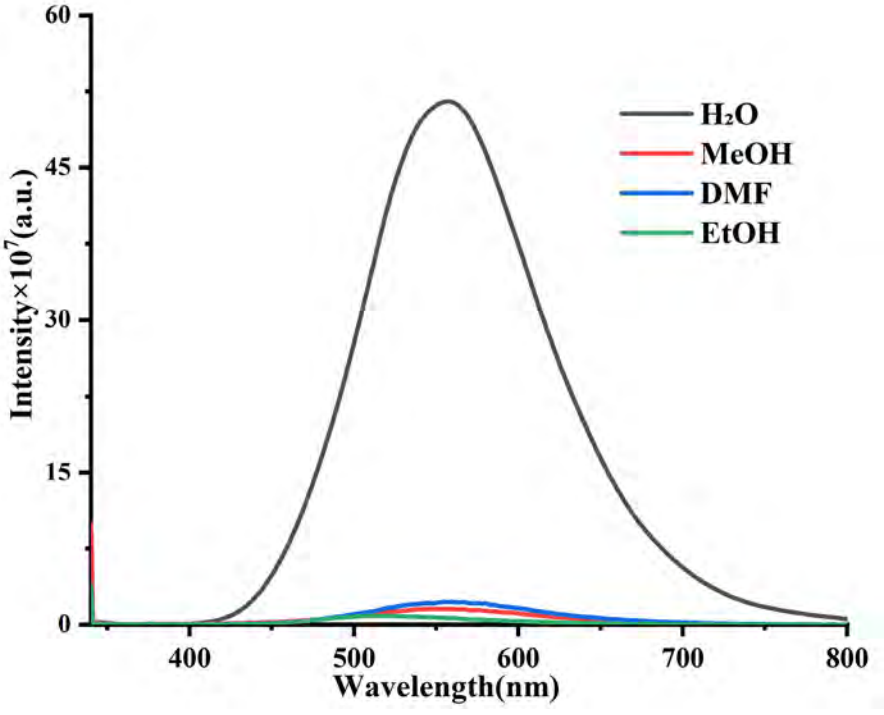

Fig. S13 The emission spectra of complex **1** dispersed in different solvents at excitation of 340 nm.

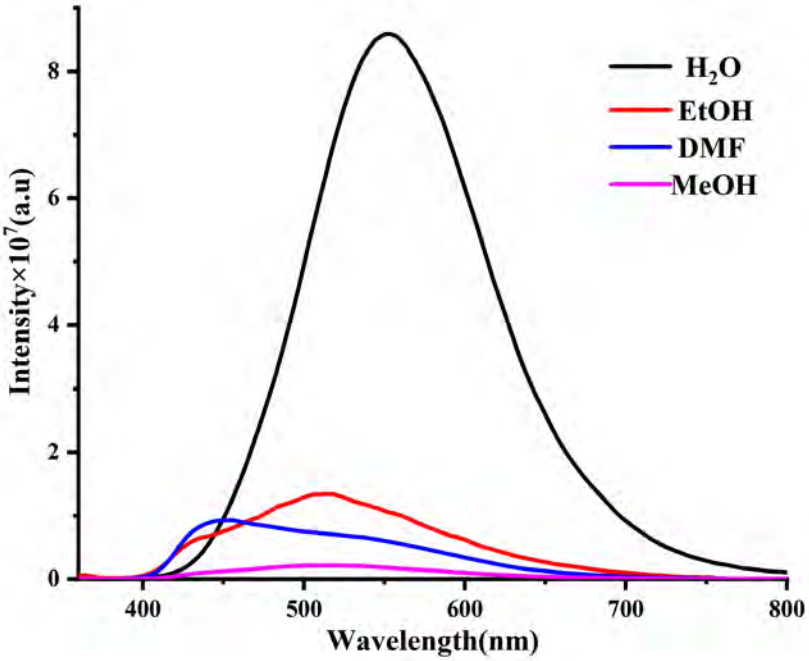

Fig. S14 The emission spectra of complex **2** dispersed in different solvents at excitation of 330 nm.

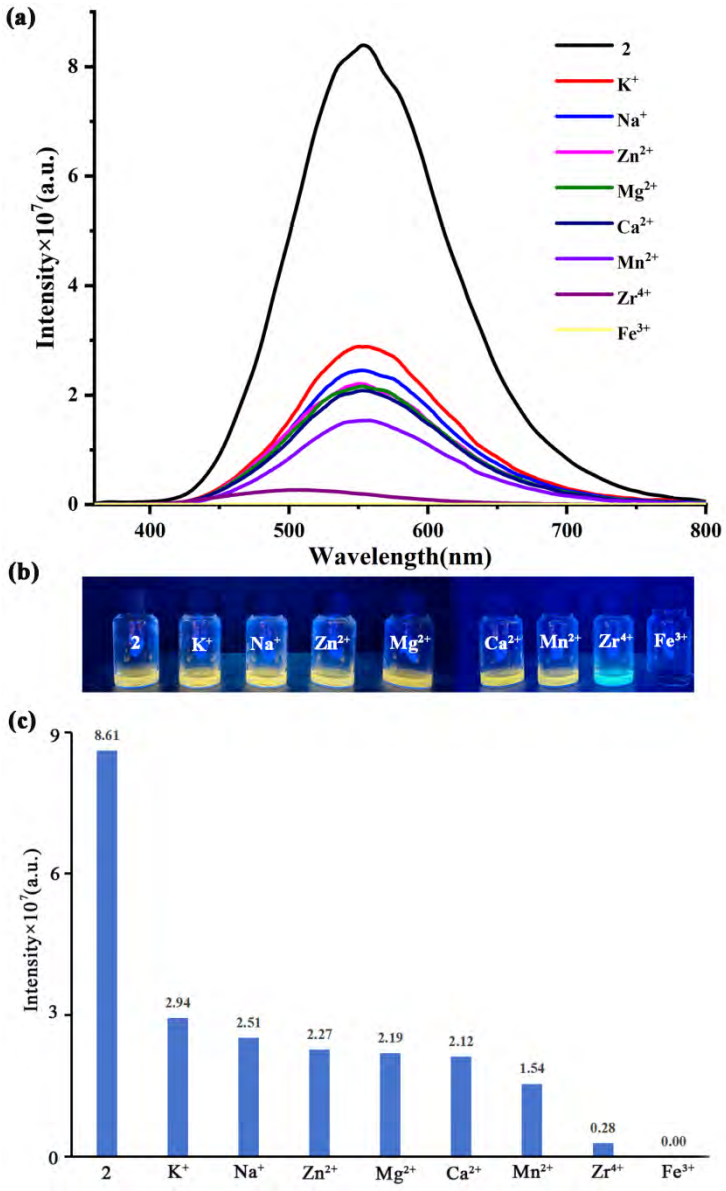

Fig. S15 (a) The emission spectra of complex **2** dispersed in different cations in H_2O at excitation of 330 nm. (b) The photographic images of complex **2** dispersed in different cation solutions. (c) Fluorescence intensities of complex **2** in different cations in H_2O.

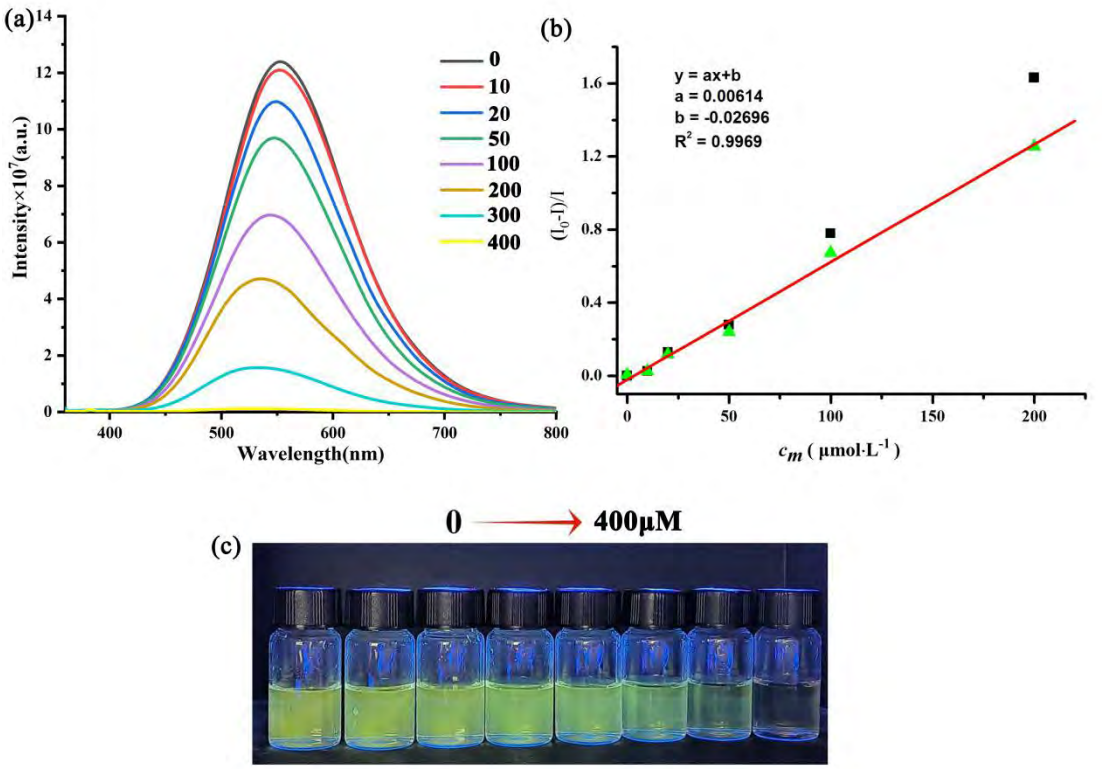

Fig. S16 (a) Fluorescence spectra of **1** dispersed in water after adding different concentration of Fe^{3+} ion solution (μM). (b) the SV plot for fluorescence intensity of **1** vs concentration of Fe^{3+} ion: black) before inner-filter correction; green) after inner-filter correction; red) the fitting for the corrected curve. (c) The photographic images of complex **1** dispersed in different concentration of Fe^{3+} ion solution.

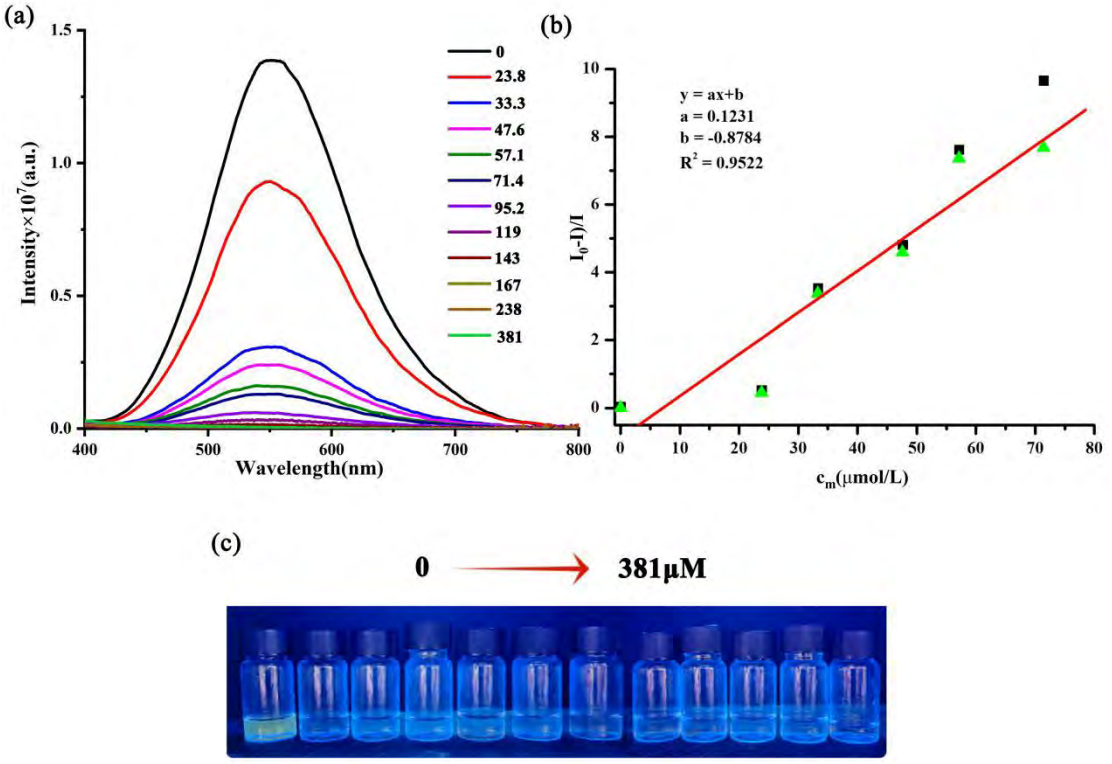

Fig. S17 (a) Fluorescence spectra of **2** dispersed in water after adding different concentration of Fe^{3+} ion solution (μM); (b) the SV plot for fluorescence intensity of **2** vs concentration of Fe^{3+} ion: black) before inner-filter correction; green) after inner-filter correction; red) the fitting for the corrected curve. (c) The photographic images of complex **2** dispersed in different concentration of Fe^{3+} ion solution.

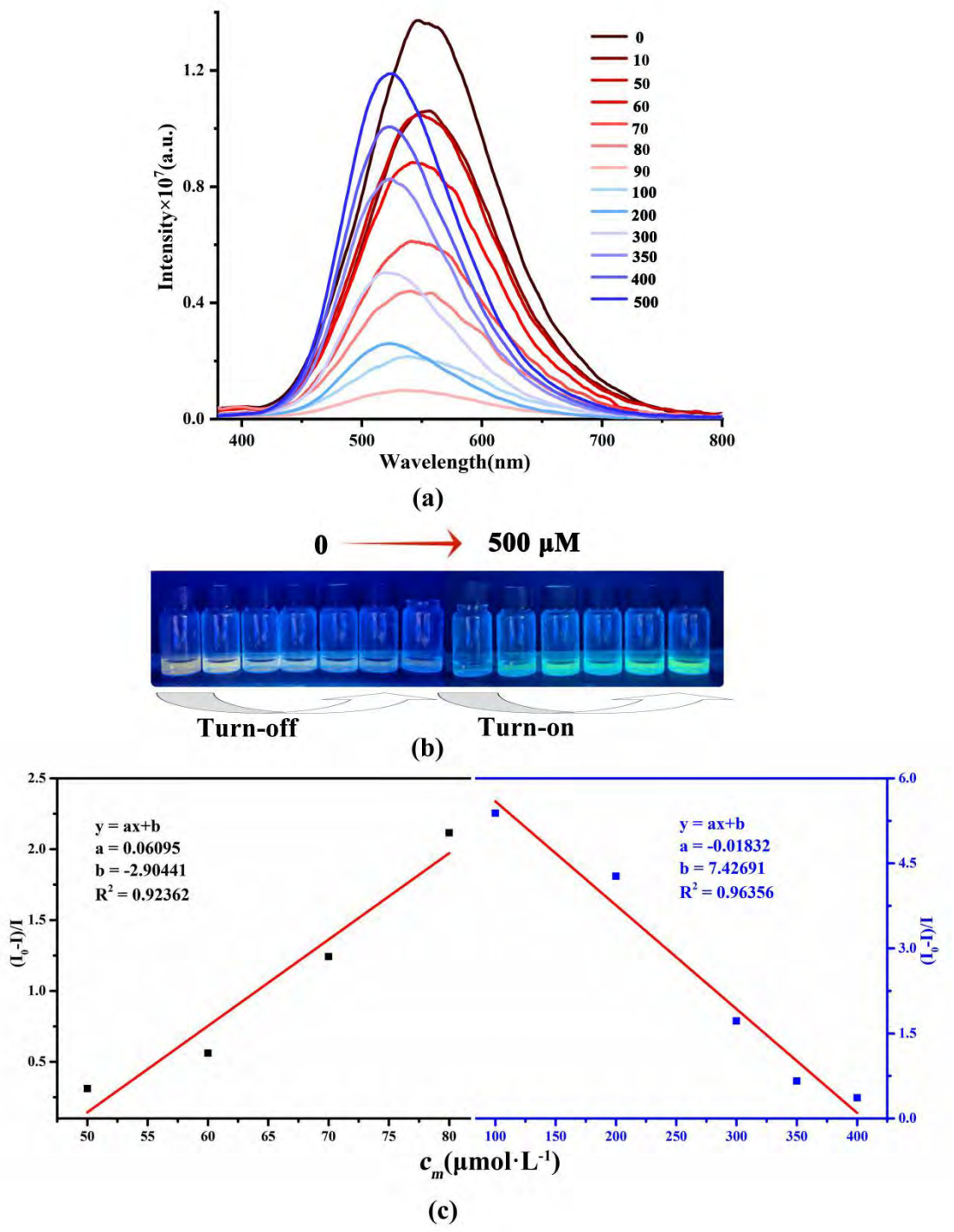

Fig. S18 (a) The emission spectra of complex **2** dispersed in different concentration of Zr^{4+} ion solution (μM) at excitation of 330 nm; (b) photos showing the turn-off and turn-on fluorescence triggered by the different volumes of Zr^{4+} ion solution; (c) the SV plot for fluorescence intensity of **2** vs concentration of Zr^{4+} ion.

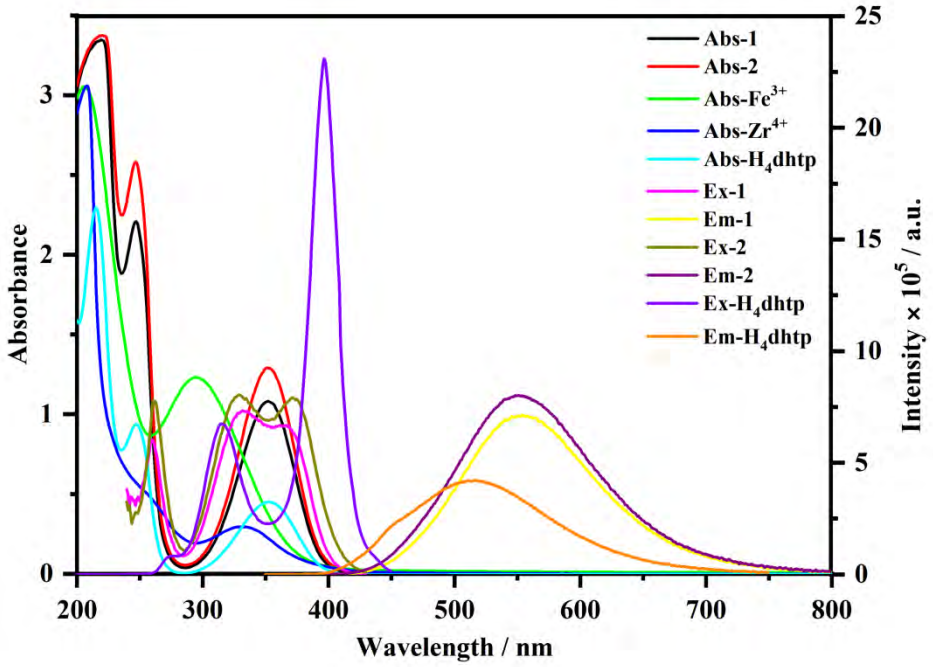

Fig. S19 The UV-Vis curves of Fe^{3+} ion, and Zr^{4+} ion. The UV-Vis, excitation spectra and emission spectra of the solution of **1**, **2**, H_4dhtp ligand, Fe^{3+} ion, and Zr^{4+} ion.

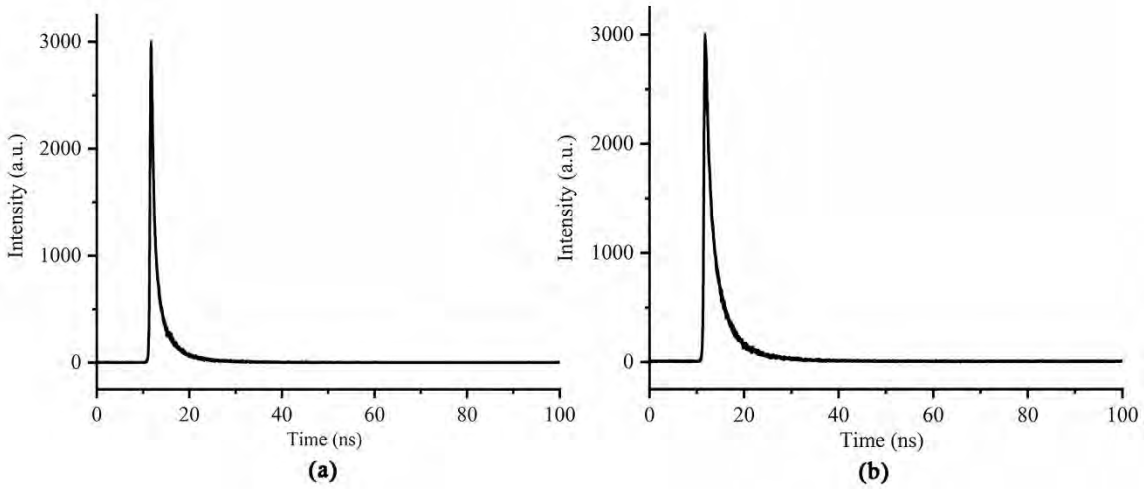

Fig. S20 Decay curves of **1** (a) and **2** (b) in the solid-state.

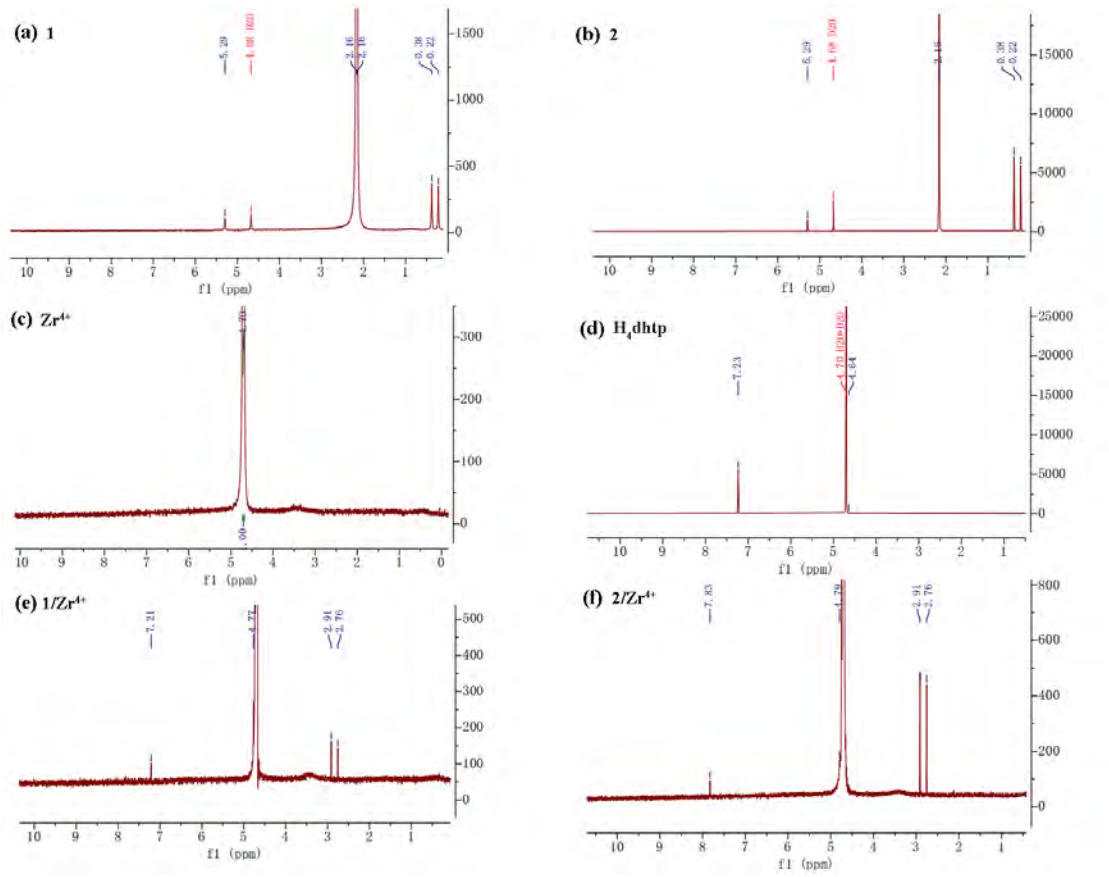

Fig. S21 The ^{1}H NMR spectrum (400 MHz, in D_2O): (a) **1** in D_2O; (b) **2** in D_2O; (c) the Zr^{4+} in D_2O; (d) the ligand H_4dhtp in D_2O; (e) **1** treated with a D_2O solution of Zr^{4+} ion (700 μM); (f) **2** treated with a D_2O solution of Zr^{4+} ion (500 μM).

Table S1 The crystallographic data for **1-2.**

	1	**2**
CCDC number	2232272	2312375
formula	$C_{36}H_{50}N_4O_{27}Tb_2$	$C_{36}H_{50}N_4O_{27}Y_2$
fw	1288.66	1148.62
space group	P-1	P-1
crystal system	triclinic	triclinic
***a*/Å**	10.8378(2)	10.7730(2)
***b*/Å**	11.3215(2)	11.2540(2)
***c*/Å**	19.7056(4)	19.6698(4)
***α*/°**	83.585(2)	83.590(2)
***β*/°**	83.958(2)	83.845(2)
***γ*/°**	79.708(2)	79.622(2)

V/Å^3	2355.07(8)	2321.80(8)
Z	2	2
calculated density (g.cm^{-3})	1.817	1.643
absorption coefficient (μ,mm^{-1})	15.419	4.201
F(000)	1280.0	1176.0
crystal size (mm^3)	0.3 × 0.2 × 0.1	0.304 × 0.185 × 0.111
2θ range (deg)	7.972 to 148.718	8.022 to 152.478
unique reflns (R_{int})	9629(0.0406)	9517(0.0293)
R_1[a], wR_2[b] ($I > 2\sigma(I)$)	0.0297, 0.0734	0.0274, 0.0663
R_1[a], wR_2[b] (all data)	0.0340, 0.0758	0.0330, 0.0693
GOF on F^2	1.021	1.046

[a] $R_1 = \sum(||F_o| - |F_c||) / \sum|F_o|$; [b] $wR_2 = \left[\sum w(|F_o|^2 - |F_c|^2)^2 / \sum w(|F_o|^2)^2\right]^{1/2}$.

Table S2 Selected bond lengths (Å) and angles (deg) for **1.**

Bond lengths [Å]			
Tb(1)-O(1)	2.312(2)	Tb(2)-O(8)#1	2.4010(19)
Tb(1)-O(17)#3	2.380(2)	Tb(2)-O(6)#1	2.361(2)
Tb(1)-O(16)	2.353(2)	Tb(2)-O(7)	2.320(2)
Tb(1)-O(2)#3	2.417(2)	Tb(2)-O(5)	2.3088(19)
Tb(1)-O(10)	2.417(2)	Tb(2)-O(14)#2	2.458(2)
Tb(1)-O(1W)	2.386(2)	Tb(2)-O(2W)	2.437(2)
Tb(1)-O(20)	2.430(2)	Tb(2)-O(4W)	2.408(2)
Tb(1)-O(19)	2.386(2)	Tb(2)-O(3W)	2.360(2)
Angles [deg]			
O(1)-Tb(1)-O(17)#3	78.49(8)	O(8)#1-Tb(2)-O(14)#2	73.08(7)
O(1)-Tb(1)-O(16)	71.87(8)	O(8)#1-Tb(2)-O(2W)	136.61(8)
O(1)-Tb(1)-O(2)#3	121.91(8)	O(8)#1-Tb(2)-O(4W)	80.07(8)
O(1)-Tb(1)-O(10)	141.11(8)	O(6)#1-Tb(2)-O(8)#1	77.68(8)
O(1)-Tb(1)-O(1W)	142.41(8)	O(6)#1-Tb(2)-O(14)#2	70.76(8)
O(1)-Tb(1)-O(20)	76.79(8)	O(6)#1-Tb(2)-O(2W)	143.06(9)
O(1)-Tb(1)-O(19)	88.96(9)	O(6)#1-Tb(2)-O(4W)	140.25(8)
O(17)#3-Tb(1)-O(2)#3	74.06(8)	O(7)-Tb(2)-O(8)#1	120.73(7)
O(17)#3-Tb(1)-O(10)	136.53(8)	O(7)-Tb(2)-O(6)#1	73.78(8)
O(17)#3-Tb(1)-O(1W)	75.46(8)	O(7)-Tb(2)-O(14)#2	137.61(8)
O(17)#3-Tb(1)-O(20)	72.89(8)	O(7)-Tb(2)-O(2W)	75.17(8)
O(17)#3-Tb(1)-O(19)	142.61(8)	O(7)-Tb(2)-O(4W)	145.75(8)
O(16)-Tb(1)-O(17)#3	128.12(7)	O(7)-Tb(2)-O(3W)	82.18(9)
O(16)-Tb(1)-O(2)#3	86.73(8)	O(5)-Tb(2)-O(8)#1	72.65(8)
O(16)-Tb(1)-O(10)	71.68(7)	O(5)-Tb(2)-O(6)#1	119.75(8)
O(16)-Tb(1)-O(1W)	145.61(8)	O(5)-Tb(2)-O(7)	78.37(8)
O(16)-Tb(1)-O(20)	135.69(8)	O(5)-Tb(2)-O(14)#2	140.34(8)

O(16)-Tb(1)-O(19)	78.83(9)	O(5)-Tb(2)-O(2W)	72.06(8)
O(2)#3-Tb(1)-O(20)	237.05(9)	O(5)-Tb(2)-O(4W)	83.53(8)
O(10)-Tb(1)-O(2)#3	68.70(8)	O(5)-Tb(2)-O(3W)	142.20(8)
O(10)-Tb(1)-O(20)	123.14(9)	O(2W)-Tb(2)-O(14)#2	124.65(8)
O(1W)-Tb(1)-O(2)#3	75.81(8)	O(4W)-Tb(2)-O(14)#2	71.44(9)
O(1W)-Tb(1)-O(10)	74.39(8)	O(4W)-Tb(2)-O(2W)	71.66(9)
O(1W)-Tb(1)-O(20)	69.95(8)	O(3W)-Tb(2)-O(8)#1	144.56(8)
O(1W)-Tb(1)-O(19)	95.56(9)	O(3W)-Tb(2)-O(6)#1	84.59(9)
O(19)-Tb(1)-O(2)#3	139.77(9)	O(3W)-Tb(2)-O(14)#2	72.16(8)
O(19)-Tb(1)-O(10)	71.12(9)	O(3W)-Tb(2)-O(2W)	71.78(9)
O(19)-Tb(1)-O(20)	69.97(9)	O(3W)-Tb(2)-O(4W)	95.26(10)

Symmetry transformations used to generate equivalent atoms: #1 1-x, 1-y, -z; #2 +x, y+1, z-1; #3 -x, 1-y, 1-z.

Table S3 Selected bond lengths (Å) and angles (deg) for **2.**

Bond lengths [Å]			
Y(1)-O(1)	2.2760(15)	Y(2)-O(8)#1	2.3773(14)
Y(1)-O(17)#3	2.3543(15)	Y(2)-O(6)#1	2.3383(15)
Y(1)-O(16)	2.3310(14)	Y(2)-O(7)	2.2941(15)
Y(1)-O(2)#3	2.3921(15)	Y(2)-O(5)	2.2822(14)
Y(1)-O(10)	2.3886(15)	Y(2)-O(14)#2	2.4400(15)
Y(1)-O(1W)	2.3499(15)	Y(2)-O(2W)	2.4095(16)
Y(1)-O(20)	2.4141(16)	Y(2)-O(4W)	2.3726(17)
Y(1)-O(19)	2.3526(17)	Y(2)-O(3W)	2.3276(15)
Angles [deg]			
O(1)-Y(1)-O(17)#3	78.37(5)	O(8)#1-Y(2)-O(14)#2	72.81(5)
O(1)-Y(1)-O(16)	72.09(5)	O(8)#1-Y(2)-O(2W)	136.83(6)
O(1)-Y(1)-O(2)#3	121.34(6)	O(6)#1-Y(2)-O(8)#1	77.02(6)
O(1)-Y(1)-O(10)	141.10(5)	O(6)#1-Y(2)-O(14)#2	70.78(6)
O(1)-Y(1)-O(1W)	142.11(5)	O(6)#1-Y(2)-O(2W)	143.40(6)
O(1)-Y(1)-O(20)	76.47(6)	O(6)#1-Y(2)-O(4W)	140.08(6)
O(1)-Y(1)-O(19)	88.53(6)	O(7)-Y(2)-O(8)#1	120.45(6)
O(17)#3-Y(1)-O(2)#3	73.68(6)	O(7)-Y(2)-O(6)#1	73.92(6)
O(17)#3-Y(1)-O(10)	136.47(5)	O(7)-Y(2)-O(14)#2	137.82(5)
O(17)#3-Y(1)-O(20)	73.14(6)	O(7)-Y(2)-O(2W)	75.21(6)
O(16)-Y(1)-O(17)#3	126.87 (5)	O(7)-Y(2)-O(4W)	145.86(6)
O(16)-Y(1)-O(2)#3	85.33 (6)	O(7)-Y(2)-O(3W)	82.29(6)
O(16)-Y(1)-O(10)	71.71 (5)	O(5)-Y(2)-O(8)#1	72.66(5)
O(16)-Y(1)-O(1W)	145.74(5)	O(5)-Y(2)-O(6)#1	119.37(6)
O(16)-Y(1)-O(20)	136.49 (6)	O(5)-Y(2)-O(7)	78.30(6)
O(16)-Y(1)-O(19)	79.51 (6)	O(5)-Y(2)-O(14)#2	140.05(5)
O(2)#3-Y(1)-O(20)	137.43(6)	O(5)-Y(2)-O(2W)	72.15(6)
O(10)-Y(1)-O(2)#3	68.99(6)	O(5)-Y(2)-O(4W)	83.39(6)

O(10)-Y(1)-O(20)	123.51(6)	O(5)-Y(2)-O(3W)	142.65(6)
O(1W)-Y(1)-O(17)#3	75.64(5)	O(2W)-Y(2)-O(14)#2	124.82(6)
O(1W)-Y(1)-O(2)#3	76.61(6)	O(4W)-Y(2)-O(8)#1	80.06(6)
O(1W)-Y(1)-O(10)	74.68(5)	O(4W)-Y(2)-O(14)#2	71.41(6)
O(1W)-Y(1)-O(20)	69.91(6)	O(4W)-Y(2)-O(2W)	71.82(6)
O(1W)-Y(1)-O(19)	95.99(6)	O(3W)-Y(2)-O(8)#1	144.19(5)
O(19)-Y(1)-O(17)#3	143.11(6)	O(3W)-Y(2)-O(6)#1	84.59(6)
O(19)-Y(1)-O(2)#3	140.21(6)	O(3W)-Y(2)-O(14)#2	72.20(5)
O(19)-Y(1)-O(10)	71.35(6)	O(3W)-Y(2)-O(2W)	72.19(6)
O(19)-Y(1)-O(20)	70.29(6)	O(3W)-Y(2)-O(4W)	95.76(7)

Symmetry transformations used to generate equivalent atoms:#1 1-x, 1-y, -z; #2 +x, 1+y, -1+z; #3 -x, 1-y, 1-z.

Table S4 The geometry analysis for complexes **1** and **2** by using SHAPE 2.1 program.

	Complex **1**		Complex **2**	
	Tb1	Tb2	Y1	Y2
OP-8 (D8h)	28.055	29.457	28.172	29.403
HPY-8 (C7v)	23.820	24.443	24.092	24.394
HBPY-8 (D6h)	16.178	15.814	16.129	15.890
CU-8 (Oh)	10.937	10.128	10.832	10.166
SAPR-8 (D4d)	1.288	1.058	1.205	1.024
TDD-8 (D2d)	1.669	1.409	1.622	1.412
JGBF-8 (D2d)	13.474	14.546	13.539	14.613
JETBPY-8 (D3h)	26.701	29.325	27.007	29.217
JBTPR-8 (C2v)	1.670	1.344	1.586	1.320
BTPR-8 (C2v)	**0.837**	**0.772**	**0.819**	**0.789**
JSD-8 (D2d)	3.826	3.656	3.747	3.619
TT-8 (Td)	11.679	10.808	11.547	10.832
ETBPY-8 (D3h)	21.761	24.937	22.070	25.017

OP-8 = Octagon; HPY-8 = Heptagonal pyramid; HBPY-8 = Hexagonal bipyramid; CU-8 = Cube; SAPR-8 = Square antiprism; TDD-8 = Triangular dodecahedron; JGBF-8 = Johnson-gyrobifastigium; JETBPY-8 = Johnson-elongated triangular bipyramid; JBTP-8 = Johnson-biaugmented trigonal prism; BTPR-8 = Biaugmented trigonal prism; JSD-8 = Snub diphenoid; TT-8 = Triakis tetrahedron; ETBPY-8 = Elongated trigonal bipyramid.

Table S5 A comparison table summarizing previously reported different materials as sensors, their Stern-Volmer quenching constants (Ksv), and Limits of Detection (LOD) for the detection of Fe^{3+}.

Materials	Ksv	LOD/ ($\mu mol \cdot L^{-1}$)	Ref.
Cd-MOF	99.351 $L \cdot mmol^{-1}$	0.89	[1]
[Tb(BTB)(DMF)]	/	10	[2]
RhB@DiCH$_3$MOF-5	/	0.36	[3]

$[Zn_2(tpt)(tda)_2]\cdot H_2O$	$4.6*10^4$ L·mmol^{-1}	4.72	[4]
Zn-MOF-74	/	1.04	[5]
Eu^{3+}@UiO-66	3.78×10^3 M^{-1},	12.8	[6]
1	0.00614 L·μmol^{-1}	31.99	This work
2	0.1231 L·μmol^{-1}	1.7	This work

1. Z. CongYi, L. QinQin, D. MingZhu, F. ChenYang, X. Ye, L. GuangZe and W. SiYu, *Chinese Journal of Inorganic Chimistry* 2023, **39** 2301-2310.
2. H. Xu, H.-C. Hu, C.-S. Cao and B. Zhao, *Inorganic Chemistry*, 2015, **54**, 4585-4587.
3. L. Guo, Y. Liu, R. Kong, G. Chen, Z. Liu, F. Qu, L. Xia and W. Tan, *Analytical Chemistry*, 2019, **91**, 12453-12460.
4. X. Zhuang, X. Zhang, N. Zhang, Y. Wang, L. Zhao and Q. Yang, *Crystal Growth & Design*, 2019, **19**, 5729-5736.
5. J. Wang, Y. Fan, H.-w. Lee, C. Yi, C. Cheng, X. Zhao and M. Yang, *ACS Applied Nano Materials*, 2018, **1**, 3747-3753.
6. L. Li, S. Shen, W. Ai, S. Song, Y. Bai and H. Liu, *Sensors and Actuators B: Chemical*, 2018, **267**, 542-548.